applied sciences

MDPI

Article

Analysis of a New Twin Hybrid Autonomous Underwater Vehicle

Jiafeng Huang [1,2], Hyeung-Sik Choi [1,*], Dong-Wook Jung [1,2], Ki-Beom Choo [1], Hyunjoon Cho [1], Phan Huy Nam Anh [1,2], Ruochen Zhang [1,2], Joon-Young Kim [3], Daehyeong Ji [4] and Jung-Hyeun Park [1,2]

[1] Department of Mechanical Engineering, Korea Maritime & Ocean University, Busan 49112, Republic of Korea
[2] Interdisciplinary Major of Ocean Renewable Energy Engineering, Korea Maritime & Ocean University, Busan 49112, Republic of Korea
[3] Department of Ocean Advanced Materials Convergence Engineering, Korea Maritime & Ocean University, Busan 49112, Republic of Korea
[4] Maritime ICT R&D Center, Korea Institute of Ocean Science and Technology, Busan 49111, Republic of Korea
* Correspondence: hchoi@kmou.ac.kr; Tel.: +82 010-5581-2971

Abstract: The twin hybrid autonomous underwater vehicle (THAUV) is a novel type of unmanned underwater platform that consists of a twin torpedo-shaped hull and is actuated by two buoyancy engines and two thrusters proposed in this paper. The THAUV was designed to have faster speed generated by the two buoyancy engines and two thrusters. The two buoyancy engines on each hull and the airfoil are mainly responsible for the diving and surfacing motion, and the thrusters drive the THAUV along the horizontal plane. The THAUV is capable of carrying more instrumentation and energy than a conventional hybrid autonomous underwater vehicle (HAUV) with a single buoyancy engine such that the THAUV can perform more exploration tasks and operate for a longer period in a one-time operation. Different from other unmanned underwater vehicles (UUVs) with two airfoils or wings, the THAUV has a single airfoil connecting the twin hull such that it does not require connecting bars and additional airfoils. For this reason, the structure of THAUV is more compact and simpler. In this paper, a new compact THAUV is designed and CFD simulation is used to obtain the hydrodynamic parameters of THAUV operation in water. The motion model of the THAUV is also established and the operating parameters of the THAUV are obtained by simulation.

Keywords: twin hybrid autonomous underwater vehicle; two buoyancy engines; compact structure; simulation

Citation: Huang, J.; Choi, H.-S.; Jung, D.-W.; Choo, K.-B.; Cho, H.; Anh, P.H.N.; Zhang, R.; Kim, J.-Y.; Ji, D.; Park, J.-H. Analysis of a New Twin Hybrid Autonomous Underwater Vehicle. *Appl. Sci.* **2023**, *13*, 1551. https://doi.org/10.3390/app13031551

Academic Editors: Minvydas Ragulskis, Wen-Hsiang Hsieh and Jia-Shing Sheu

Received: 1 December 2022
Revised: 10 January 2023
Accepted: 20 January 2023
Published: 25 January 2023

1. Introduction

Underwater gliders (UG), autonomous underwater vehicles (AUV), and remotely operated vehicles (ROV) [1–3] have been developed for decades as major underwater monitoring platforms. Compared with ROV, AUV are untethered, pre-programmed operating platforms, which means they have a wider working envelope and longer mission cycles [4]. UG is a monitoring system driven by buoyancy, which makes UG possess the characteristics of low energy consumption and longer working time. In the literature, [5] studied a vertically aligned two-compartment autonomous underwater vehicle and performed motion simulations. The hybrid autonomous underwater vehicle (HAUV) combines the advantages of low energy consumption of UG and strong mobility of AUV, alternating the working modes of UG and AUV to complete a wide range of underwater data collection and subsea monitoring. In reference [6], a nonlinear kinematic and dynamic model of a hybrid autonomous underwater vehicle (HAUV) is derived for the two modes of locomotion, namely, propelled (AUV) and gliding (UG) modes. The HAUV adopts the UG operation mode in the process of underwater data acquisition, i.e., by adjusting the magnitude and direction of buoyancy to make it alternately operate underwater diving and surfacing. It can also adjust the buoyancy to make it hover horizontally and use thrusters

to drive it to complete the acquisition of data such as seafloor topography. After finishing the sampling work in a certain water area, the AUV mode is used to change the course to the next collection region. The THAUV is a kind of HAUV with two buoyant bodies. The fixed wing plays a vital role in the work of the UG and the HAUV; the lift generated by the wing drives the UG and HAUV forward during the dive and surfacing states and CFD numerical calculations are used to study the hydrodynamic characteristics of torpedo-type underwater gliders. [7]. The acquisition of hydrodynamic parameters is crucial to the simulation prediction of the UG and the HAUV. Common methods include the experimental method, parameter identification method, and computational fluid dynamic (CFD) simulation. The hydrodynamic performance and parameters of the underwater glider were calculated using experimental methods as described in reference [8]. In reference [9], the authors described the identification of model parameters for SLOCUM using experimental flight test data. In particular, the focus is on data from a steady linear glide. CFD is widely used for the calculation of hydrodynamic parameters of underwater equipment because of its low cost and fast result acquisition. The application of CFD methods for modeling and hydrodynamic analysis of underwater gliders is described in detail in Reference [10].

The operating modes of this THAUV can be divided into two types according to the operating mechanism, i.e., glide mode and AUV mode. In the glide mode, the net buoyancy and the position of the center of gravity are regulated by the displacement change of the piston, which drives the glider to move downward (gravity over buoyancy) or move upward (buoyancy over gravity) in the vertical plane. In AUV mode, the piston is adjusted to keep the glider in a neutral state, and the thruster is used to drive the glider to move in the horizontal plane for tasks such as target search and seafloor scanning, while the elevator is responsible for adjusting the attitude of the glider to keep it horizontal (the angle of attack is 0). In this paper, the gliding mode is taken as the research objective, and suitable airfoil selection is obtained through simulation of the gliding motion.

2. Structure of THAUV

The twin hybrid autonomous underwater vehicle (THAUV) is a new type of underwater monitoring platform with two buoyant bodies, which allows it to carry more energy and a variety of measurement equipment. The two buoyant bodies are connected by an aluminum plate, which can also be considered as a fixed wing of the THAUV. In order to reduce the resistance to underwater movement, the main body of the THAUV is a torpedo-shaped rotating body. The rotating body is modeled using the MYRING hull profile equations [11], and the overall structural diagram of the THAUV is shown in Figure 1.

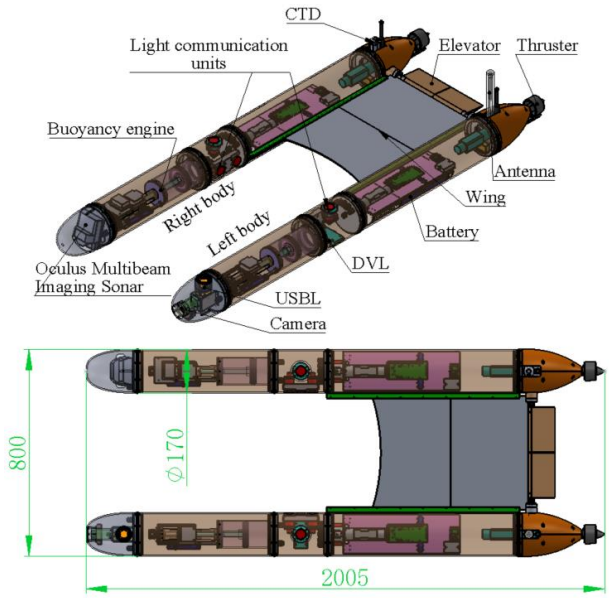

Figure 1. The structure of the THAUV.

The mass of the entire THAUV system consists of two parts: the dynamic mass, including the mass of the piston ($m_p = 1.022$), the mass of the ballast water (m_b), and the static mass ($m_s = 65.33$), which is the sum of the mass of the roller ($m_r = 1.04$), and the mass of the remaining static accessories ($m_{sb} = 64.29$). Due to the limited rotation range of the elevator, the effect of the elevator on the floating center and center of gravity is negligible. The mass distribution is illustrated in Figure 2.

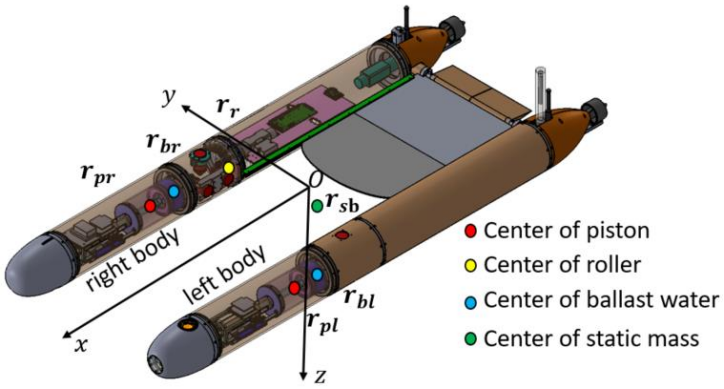

Figure 2. Mass distribution and descriptions.

The total mass of the THAUV is expressed in Equation (1):

$$m = m_p + m_s = m_{pr} + m_{pl} + m_r + m_{sb} \tag{1}$$

The derived equation for the center of gravity is shown in Equation (2):

$$\boldsymbol{r}_{CG} = \left[m_{pr}\boldsymbol{r}_{pr} + m_{pl}\boldsymbol{r}_{pl} + m_s\boldsymbol{r}_s\right]/m \tag{2}$$

$$\boldsymbol{r}_s = (m_r\boldsymbol{r}_r + m_{sb}\boldsymbol{r}_{sb})/m_s \tag{3}$$

Here $\boldsymbol{r}_{pr}$ and $\boldsymbol{r}_{pl}$ are the positions of the right and left pistons in the body coordinates, respectively; $\boldsymbol{r}_s$ is the position of static mass (including roller); $\boldsymbol{r}_r$ is the position of the roller in the body coordinates; and $\boldsymbol{r}_{sb}$ is the equivalent position of the remaining static accessories in the body coordinates (it is a fixed value).

Since the roller only rotates around the axis of the right body shown in Figure 2 and there is no displacement change in the x-axis direction, the position in the x-axis direction is fixed. Figure 3 shows the schematic diagram after the roller rotation angle γ.

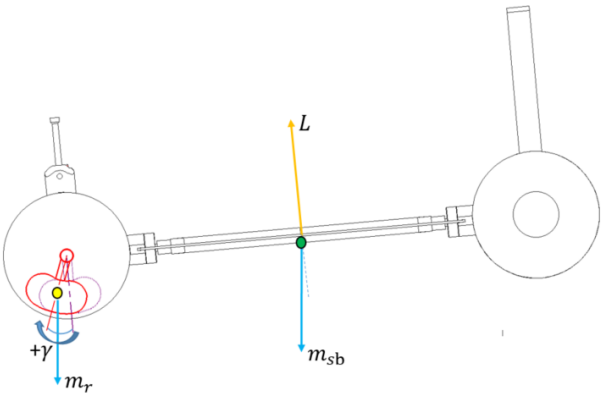

Figure 3. Schematic diagram of roller rotation.

At this time, the center of gravity is shifted in the y-axis direction, resulting in the tilting of the body in the y-axis, and the THAUV will produce a rotary hovering motion around a certain point due to the action of hydrodynamic lift. When the rotation angle of the roller is γ, the position coordinates of the roller can be expressed as:

$$\boldsymbol{r}_r = r_{rxi}\begin{bmatrix}1\\0\\0\end{bmatrix} + \left(r_{ryi} + R_r sin\gamma\right)\begin{bmatrix}0\\1\\0\end{bmatrix} + \left[r_{rzi} - \left(R_r - R_r cos\gamma\right)\right]\begin{bmatrix}0\\0\\1\end{bmatrix} \tag{4}$$

Here, R_r is the radius of rotation of the roller center of mass and r_{rxi}, r_{ryi}, and r_{rzi} are the initial coordinates of the roller in the body coordinates along the x,y,z axis, respectively, when the roller does not rotate.

In this design, the buoyancy engine adopts the structure of piston, which changes the magnitude and direction of the net buoyancy of the THAUV through the movement of the piston to absorb or drain water. When the piston absorbs water inward, the gravity is greater than the buoyancy, and the THAUV is diving; when the piston drains water outward, the buoyancy is greater than the gravity, and the THAUV is surfacing. In order to keep the glider balanced and stable, the ballast water in the two buoyancy engines is always equal in the absence of special requirements. The ballast water is expressed with Equation (5):

$$m_b = \rho\pi r^2 d_p, \tag{5}$$

Here, ρ is the density of the water, r is the radius of the piston ($r = 0.05$ m), and d_p is the displacement of the piston along the x-axis. Therefore, the expression of the buoyancy force of the THAUV is shown below:

$$m_B = M_B - 2m_b \tag{6}$$

Here, m_B is the maximum displacement mass of THAUV.

The buoyancy center is derived with Equation (7):

$$\boldsymbol{r}_{CB} = -m_b\left(\boldsymbol{r}_{pr} + \boldsymbol{r}_{pl}\right)/m_B \tag{7}$$

3. Mathematic Model

In order to analyze the motion of the THAUV underwater, the coordinate system of the THAUV's motion was established as shown in Figure 4. The coordinate system includes a reference coordinate system E-XYZ and body coordinate system O-xyz, with the buoyancy

center of the THAUV as the coordinate origin, in addition to the velocity coordinate system $\boldsymbol{\pi}_0$ of the THAUV's motion.

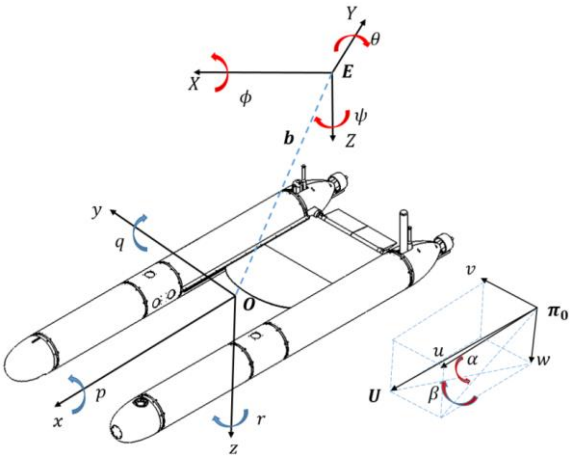

Figure 4. Coordinate system of the THAUV.

The position and attitude of the THAUV in the inertial coordinate system can be expressed as $\mathbf{b} = \begin{bmatrix} x & y & z \end{bmatrix}^T$ and $\boldsymbol{\Omega} = \begin{bmatrix} p & q & r \end{bmatrix}^T$. The linear and angular velocities of the THAUV in the body coordinate system can be expressed as $\mathbf{V} = \begin{bmatrix} u & v & w \end{bmatrix}^T$ and $\boldsymbol{\omega} = \begin{bmatrix} p & q & r \end{bmatrix}^T$. The rotation matrix from the body frame to the inertial frame is $\mathbf{R}$.

$$\mathbf{R} = \begin{bmatrix} cos\psi\cos\theta & -sin\psi cos\phi + cos\psi sin\theta sin\phi & sin\psi sin\phi + cos\psi cos\phi sin\theta \\ sin\psi cos\theta & cos\psi cos\phi + sin\phi sin\theta sin\psi & -cos\psi sin\phi + sin\theta sin\psi cos\phi \\ -sin\theta & cos\theta sin\phi & cos\theta cos\phi \end{bmatrix} \tag{8}$$

Then, the kinematic equation of the THAUV can be expressed as:

$$\dot{\boldsymbol{b}} = \boldsymbol{RV} \tag{9}$$

$$\dot{\boldsymbol{R}} = \boldsymbol{R}\hat{\boldsymbol{\omega}} \tag{10}$$

A detailed derivation of the kinetic equations of the underwater glider is given in the literature [12,13]. Referring to the above literature, the equations of motion governing a THAUV propagating in a three-dimensional space are expressed as:

$$\begin{bmatrix} \dot{\mathbf{R}} \\ \dot{\mathbf{b}} \\ \dot{\mathbf{v}} \\ \dot{\boldsymbol{\omega}} \\ \dot{\boldsymbol{r}}_p \\ \dot{\mathbf{P}}_p \\ \dot{\mathbf{P}}_p \\ \dot{\mathbf{m}}_0 \end{bmatrix} = \begin{bmatrix} \mathbf{R}\hat{\boldsymbol{\omega}} \\ \mathbf{Rv} \\ \boldsymbol{M}^{-1}\boldsymbol{F} \\ \boldsymbol{J}^{-1}\boldsymbol{\tau} \\ \dot{\boldsymbol{d}}_p \\ m_p\left(\mathbf{v} + \boldsymbol{\omega} \times \boldsymbol{r}_p + \dot{\boldsymbol{r}}_p\right) \\ \mathbf{u}_p \\ \mathbf{u}_0\dot{\boldsymbol{d}}_p \end{bmatrix} \tag{11}$$

The total moment and force are expressed as follows:

$$\boldsymbol{\tau} = \left(\boldsymbol{J\omega} + \hat{\boldsymbol{r}}_p\mathbf{P}_p\right) \times \boldsymbol{\omega} + \boldsymbol{M}\mathbf{v} \times \mathbf{v} + \boldsymbol{\omega} \times \boldsymbol{r}_p \times \mathbf{P}_p + m_p\hat{\boldsymbol{r}}_p\mathrm{g}\boldsymbol{R}^{\boldsymbol{T}}\boldsymbol{k} + \boldsymbol{\tau_{ext}} - \hat{\boldsymbol{r}}_p\mathbf{u}_p \tag{12}$$

$$F = \left(\boldsymbol{M}\mathbf{v} + \mathbf{P}_p\right) \times \boldsymbol{\omega} + m_0\mathrm{g}\boldsymbol{R}^{\boldsymbol{T}}\boldsymbol{k} + \boldsymbol{F_{ext}} - \mathbf{u}_p \tag{13}$$

Here, $\boldsymbol{\tau_{ext}}$ includes the hydrodynamic moment and thruster torque, and $\boldsymbol{F_{ext}}$ includes the hydrodynamic forces and thrust of thrusters.

The THAUV in this paper can not only perform pitching motion in the vertical plane, but it can also change the heading in the horizontal direction by using the thrusters and achieve gyratory motion by controlling the deflection angle of the roller. In this paper, we focus on the pitch motion attitude of the THAUV, where the thruster, roller, and elevator remain stationary during the pitch motion. Then, the equations of the motion of the THAUV in the vertical plane can be simplified as:

$$\dot{\mathrm{x}} = \mathrm{v}_1 cos\theta + \mathrm{v}_3 sin\theta \tag{14}$$

$$\dot{\mathrm{z}} = -\mathrm{v}_1 sin\theta + \mathrm{v}_3 cos\theta \tag{15}$$

$$\dot{\theta} = \omega_2 \tag{16}$$

$$\dot{\mathrm{v}}_1 = \frac{1}{\mathrm{m}_1}\left[\left(-\mathrm{m}_3\mathrm{v}_3\omega_2 - \mathrm{P}_{p3}\omega_2\right) - \mathrm{m}_0 g sin\theta + (Lsin\alpha - \mathrm{Dcos}\alpha) - \mathrm{u}_{p1}\right] \tag{17}$$

$$\dot{\mathrm{v}}_3 = \frac{1}{\mathrm{m}_3}\left[\left(-\mathrm{m}_1\mathrm{v}_1\omega_2 + \mathrm{P}_{p1}\omega_2\right) + \mathrm{m}_0 g cos\theta - (Lcos\alpha + \mathrm{Dsin}\alpha) - \mathrm{u}_{p3}\right] \tag{18}$$

$$\begin{aligned}\dot{\omega_2} = \tfrac{1}{\mathrm{J}_2}[(\mathrm{m}_3 - \mathrm{m}_1)\mathrm{v}_1\mathrm{v}_3 - \left(r_{p1}\mathrm{P}_{p1} + r_{p3}\mathrm{P}_{p3}\right)\omega_2 - mg(r_{rx}\cos\theta + r_{rz}\sin\theta)\\ + M_{DL} - r_{p3}\mathrm{u}_{p1} + r_{P1}\mathrm{u}_{P3}]\end{aligned} \tag{19}$$

$$\dot{r}_{p1} = \dot{d}_{p1} \tag{20}$$

$$\mathrm{P}_{p1} = m_p\left(\mathrm{v}_1 + \omega_2 r_{p3} + \dot{d}_{p1}\right) \tag{21}$$

$$\mathrm{P}_{p3} = m_p\left(\mathrm{v}_3 - \omega_2 r_{p1}\right) \tag{22}$$

$$\dot{\mathrm{P}}_{p1} = u_{p1} \tag{23}$$

$$\dot{\mathrm{P}}_{p3} = u_{p3} \tag{24}$$

$$\dot{\mathrm{m}}_0 = \mathrm{u}_0\dot{d}_{p1} \tag{25}$$

$$\alpha = \ \mathrm{acrtan}\frac{\mathrm{v}_3}{\mathrm{v}_1} \tag{26}$$

$$\zeta = \ \theta - \alpha \tag{27}$$

Here, x and z are the horizontal and vertical displacements of the THAUV in the inertial frame, respectively; α is the angle of attack; θ is the pitching angle; ζ is the gliding angle; v_1 and v_3 are the velocity components of the THAUV along the x- and z-axes in the body frame, respectively; ω_2 represents the pitch angular velocity of the THAUV rotating around the y-axis of the body frame; L is the hydrodynamic lift; D is the hydrodynamic drag; M_{DL} represents the pitching moment yielded by the hydrodynamic analysis; m_1 and m_3 represent the added mass along the x- and z-axes, respectively; J_2 represents the moment of inertia rotating around the y-axis; and P_{P1}, P_{P3} represent the momenta of the piston along the x- and z-axes, respectively.

Table 1 shows a detailed description of the parameters used in the previous equations and Table 2 presents the values of each case.

Table 1. Descriptions of parameters of the above equations.

Term	Description
x	The horizontal displacement in the vertical plane
z	The vertical displacement in the vertical plane
v_1	The velocity of the glider along the x-axis in the body-fixed frame
v_3	The velocity of the glider along the z-axis in the body-fixed frame
θ	The angle of pitch
ω_2	The pitch angular velocity rotating around the y-axis of the body-fixed frame
m_1	The mass of the glider (with added mass) in the x-axis
m_3	The mass of the glider (with added mass) in the z-axis
p_{p1}	The momenta of the piston along the x-axis
p_{p3}	The momenta of the piston along the z-axis
m_0	Net buoyancy mass
L	Hydrodynamic lift
D	Hydrodynamic drag
α	Angle of attack
u_{p1}	The force acting on the piston in the x -direction
u_{p3}	The force acting on the piston in the z -direction
J_2	The moment of inertia rotating around the y-axis (without moveable mass and piston)

Table 1. *Cont.*

Term	Description
r_{p1}	Position of the piston in the x direction
r_{p3}	Position of the piston in the z direction
m	Mass of the glider
r_{rx}	Position of the gravity center in the x direction
r_{rz}	Position of the gravity center in the z direction
M_{DL}	Hydrodynamic moment
d_{p1}	The displacement of the piston along the x direction
u_0	The ballast water per meter
ζ	Gliding angle
m_p	Mass of the piston
J	The total moment of inertia of the glider rotating around the y-axis
m_s	Mass of static equilibrium
ρ	Density of the water
r	Radius of the piston
M_B	Maximum buoyancy of the glider

Table 2. Values of the THAUV.

Term	Case 01	Case 02	Case 03
$m\ (kg)$	67.37	67.02	66.3
$m_p\ (kg)$	1.022	1.022	1.022
$\mathrm{m_s}\ (kg)$	65.33	64.98	64.256
r (m)	0.05	0.05	0.05

4. Hydrodynamic Analysis

When underwater equipment works in the water, it is mainly affected by buoyancy and the hydrodynamic force generated by the relative movement of the water around the body in the process of movement. Compared with the buoyancy, the calculation of hydrodynamic force is not easy; however, it is very critical. Currently, three methods are usually used to calculate the hydrodynamic force of water-related equipment, i.e., for the target with a regular shape, the empirical formula is mostly used to predict the hydrodynamic force; for the equipment with a simple structure and low manufacturing cost, the method of the proportional model experiment is often used to obtain the hydrodynamic parameters directly; however, for the equipment with a complex structure and high manufacturing cost, the above method cannot accurately and effectively calculate the hydrodynamic force of the target. For such cases, ANSYS Fluent [14] software is used to calculate the hydrodynamic parameters of the target.

The hydrodynamic drag force of the THAUV was simulated using Fluent in this paper. The simulation domain is a rectangular body and the dimensions of the simulation domain are: 14 m in length, 6m in both width and height, and the inlet of the simulation domain is 5 m away from the floating center of the THAUV. The k-omega SST model [15] is selected as the turbulence model for this simulation and the SST model is widely used for underwater equipment simulation analysis. Due to the complexity of the THAUV tail structure, a non-structural grid is used for hydrodynamic simulation in this paper, with a total grid number of about 3,790,000 and a Yplus less than 1 [16]. The created grid is shown in Figure 5.

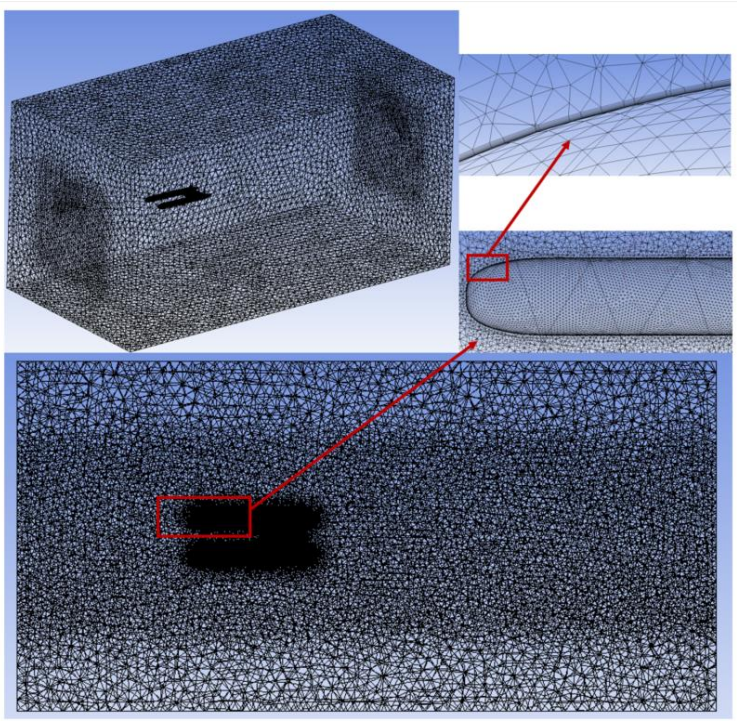

Figure 5. Non-structural grid of the CFD simulation.

In order to ensure that the number of meshes can meet the accuracy of the simulation results, the comparison of the simulation results of different meshes in the state of the THAUV with an angle of attack of +2 degrees and a gliding speed of 0.5 m/s can be obtained from the verification results of the mesh independence [17] shown in Figure 6. The grid numbers used in the figure are 2,250,000, 3,330,000, 3,790,000, and 75,200,000. In view of the simulation results, simulation time, and computer performance, the number of meshes used in this paper is about 3,790,000.

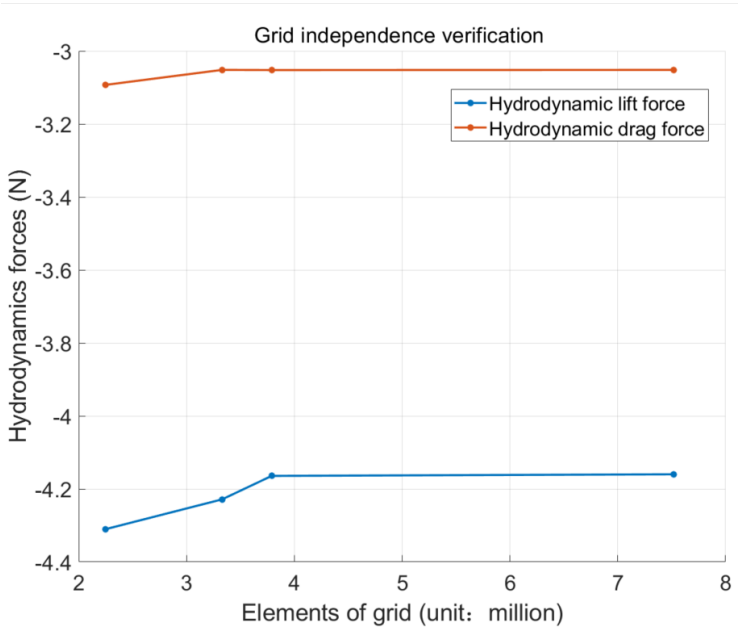

Figure 6. Grid independence verification.

In this paper, the effect of the hydrodynamics of three different sizes of fixed wing on the movement of the THAUV underwater is studied, and the three cases are shown in Figure 7 below.

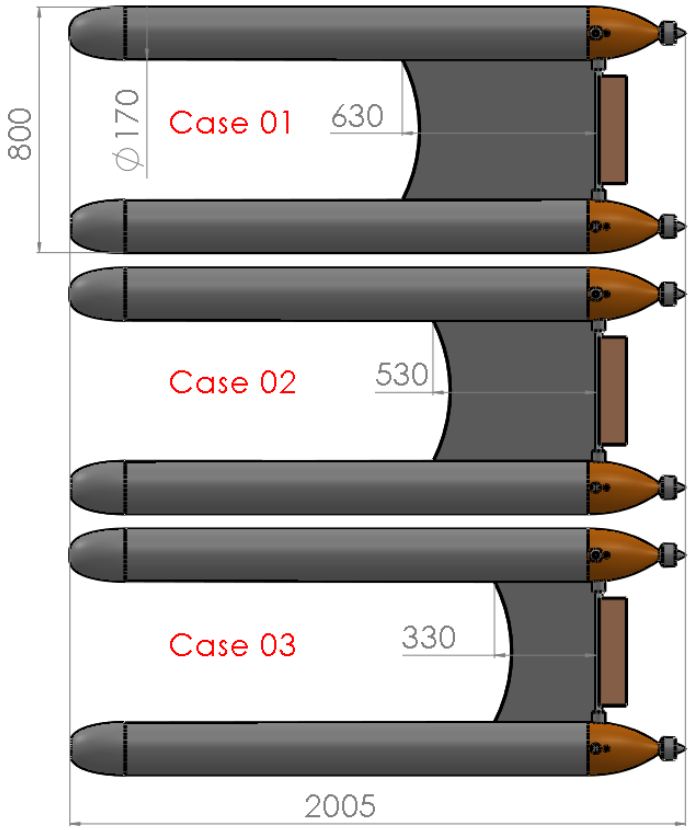

Figure 7. Three cases with different wing sizes.

The hydrodynamic lift, drag, and moment are shown in Figures 8–10 below. The trend of the values shown in the graphs shows that when the angle of attack and the velocity increase, the hydrodynamic lift, drag, and moment will also increase; the lift and moment increase almost linearly, while the growth trend of the hydrodynamic drag is in line with the quadratic growth. Since the three cases have similar hydrodynamic trends, only the graphs of hydrodynamic changes for Case 01 are shown here.

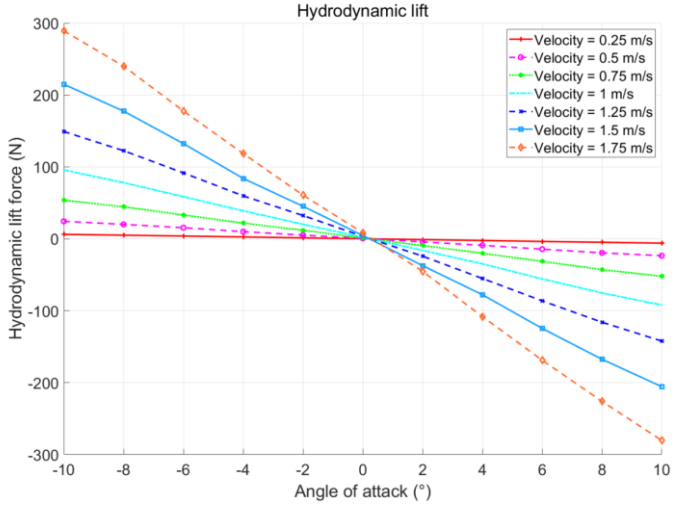

Figure 8. Hydrodynamic lift.

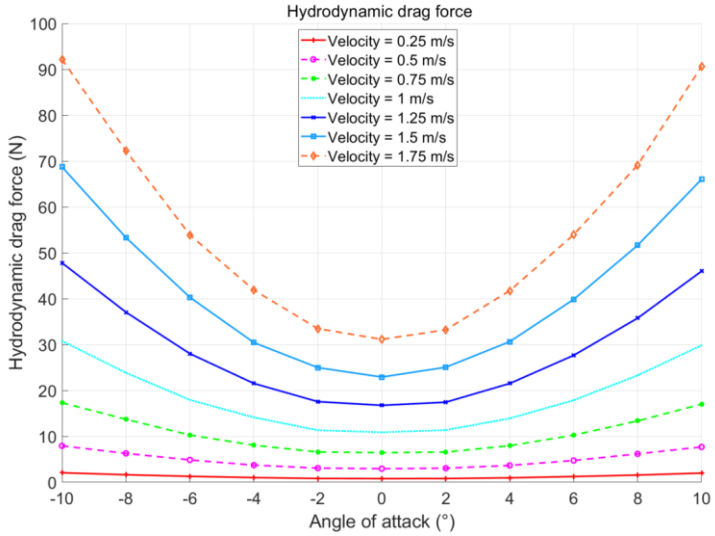

Figure 9. Hydrodynamic drag.

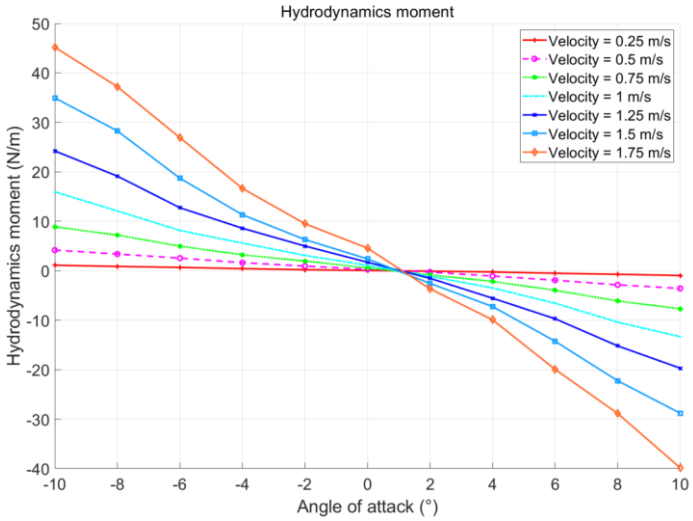

Figure 10. Hydrodynamic moment.

From the trend of hydrodynamic forces and moment shown above, it can be seen that the hydrodynamic lift (L) and moment (M_{DL}) can be expressed as a linear function of the angle of attack (α), and the hydrodynamic resistance (D) can be expressed as a quadratic function equation of the angle of attack. These expressions are shown as follows:

$$\mathrm{L} = (K_{L0} + K_L\alpha)V^2 \tag{28}$$

$$\mathrm{D} = \left(K_{D0} + K_D\alpha^2\right)V^2 \tag{29}$$

$$M_{DL} = (K_{M0} + K_M\alpha)V^2 \tag{30}$$

Here, K_s are the corresponding hydrodynamic parameters and their values are shown in the following Table 3.

Table 3. Values of hydrodynamic parameters.

	K_{L0}	K_L	K_{D0}	K_D	K_{M0}	K_M
Case 01	−1.9169	9.5281	11.1159	0.215	1.1025	−1.4179
Case 02	−1.8461	9.8351	11.5594	0.2445	0.3720	−2.4335
Case 03	−1.265	8.0948	11.2805	0.20525	0.0985	−2.8938

A comparison of hydrodynamic lift and drag relative to cruising velocity of the THAUV when it is in the AUV mode of horizontal cruise is shown in the figure below. Figures 11 and 12 show the relationship between the hydrodynamic lift and drag of the THAUV in the horizontal plane relative to the cruising speed, respectively. It can be concluded from the plot of drag that the wing area has a relatively small effect on drag as it decreases, since the buoyant body is the main factor in drag generation.

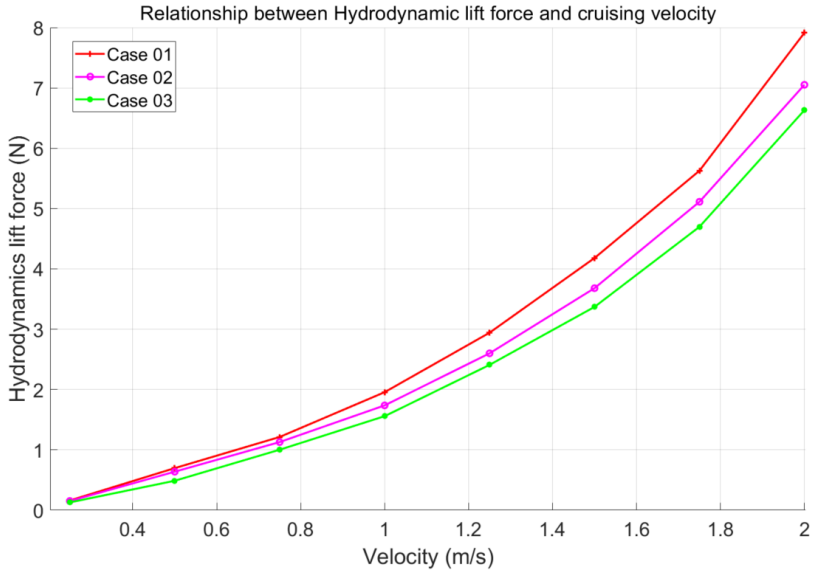

Figure 11. Variation of hydrodynamic lift with velocity.

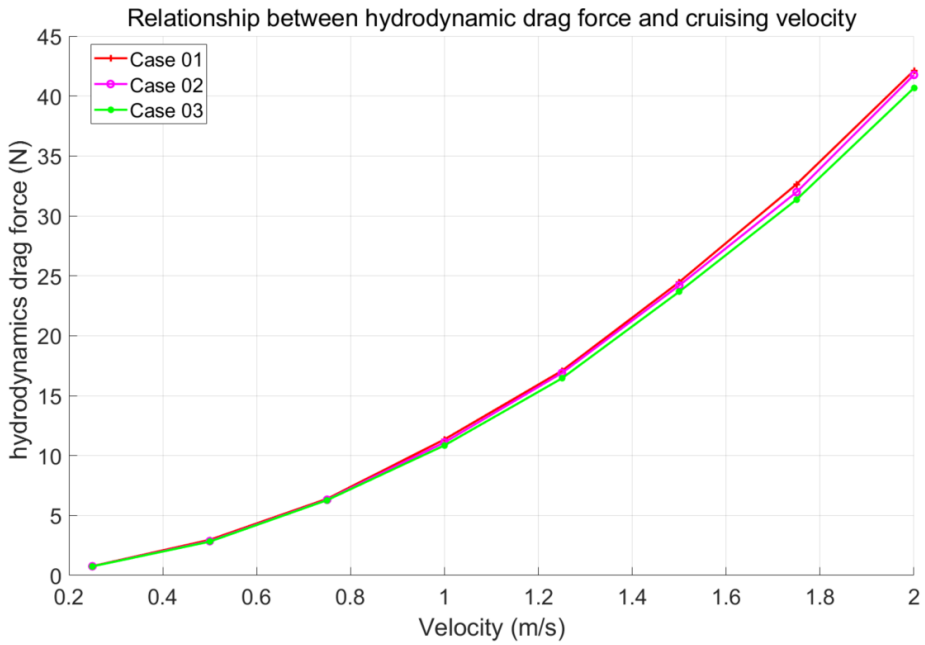

Figure 12. Variation of hydrodynamic drag with velocity.

5. Results

Based on the modeling of the aforementioned Equations (14)–(27) of motion in Section 3, this chapter mainly shows the simulation results of the THAUV within the vertical water column. The prerequisites for the simulations shown in this paper are that the roller, thruster, and elevator are at rest, mainly to show the effect of the buoyancy engine on the glide angles, and the simulation results can also be used as a reference for the actual underwater experiments. In this paper, the motion of the piston is used as the only control input.

The simulation results of the THAUV for the three cases in two working cycles (dive and then surfacing, then dive and surfacing again) are shown in Figures 13–15. During the first stage of diving and surfacing, the displacement of the piston is plus or minus 0.03 m, i.e., the change in the mass of the ballast water is plus or minus 483 g. The positive sign indicates that the buoyancy engine absorbs water inward and the buoyancy of the THAUV decreases. During the second stage of diving and surfacing at the time of 1060 s and 1430s, the displacement of the piston is plus or minus 0.05m. Figure 16 presents the comparison of the angle of attack (AoA) for the three cases.

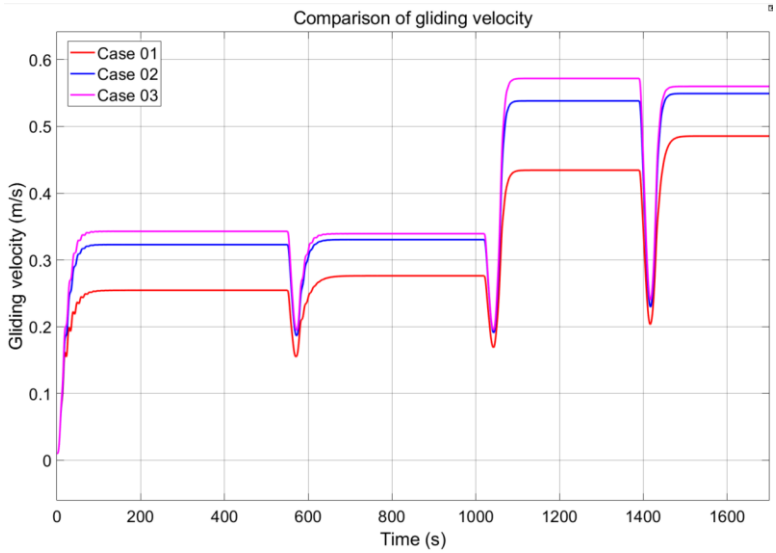

Figure 13. Comparison of gliding velocity.

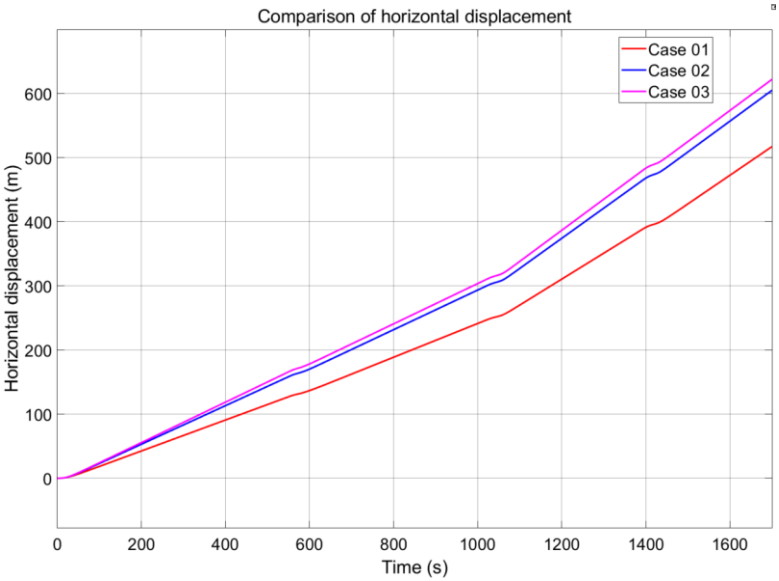

Figure 14. Comparison of horizontal displacement.

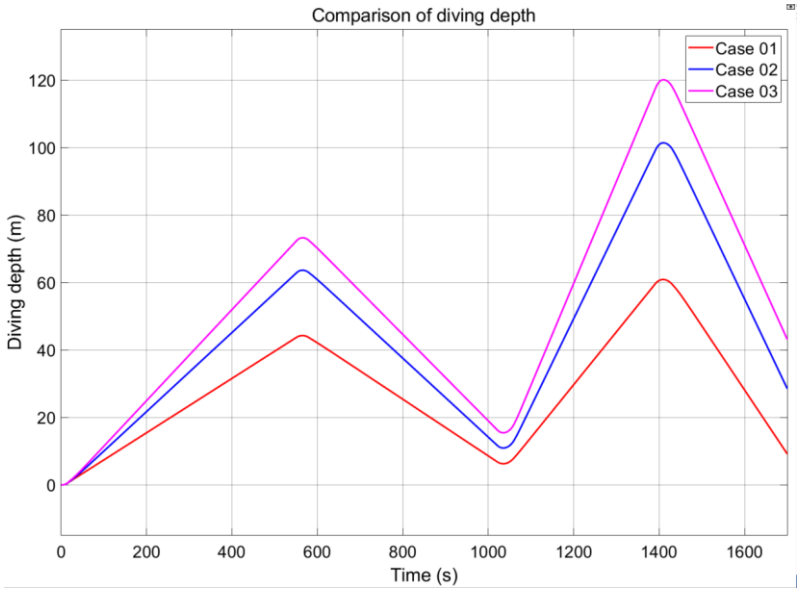

Figure 15. Comparison of diving depth.

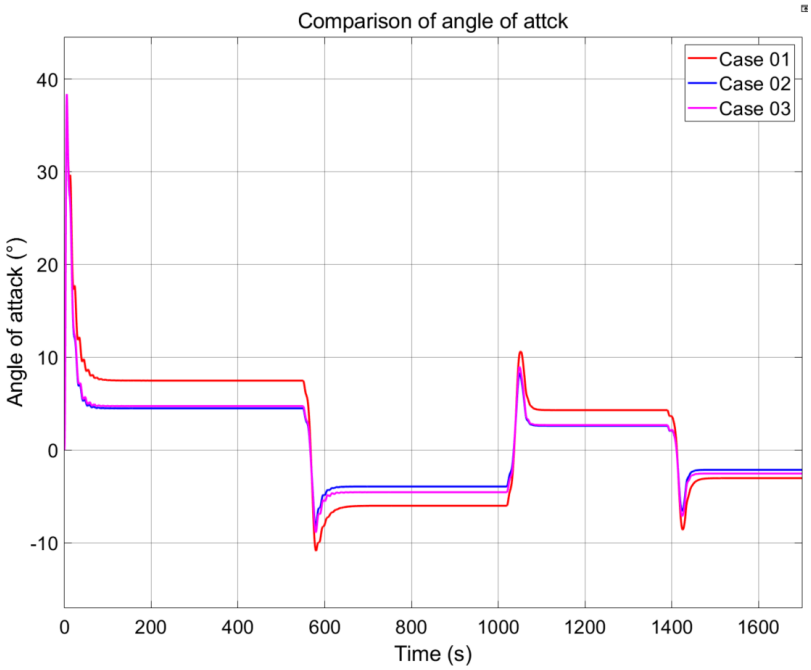

Figure 16. Comparison of AOA.

From the above comparison results, it is clear that the gliding performance of the THAUV is enhanced when the fixed wing size decreases. From the trend of the gliding performance, it can be inferred that the gliding performance will not change any more when the fixed wing size decreases to a specific value. From the curve of glide velocity, we can find that the THAUV reached the stable dive state at around 170s, and the dive velocities of Cases 01, 02, and 03 were 0.25m/s, 0.32m/s, and 0.34m/s, respectively. In the second dive stage of the THAUV, when the THAUV reached the stable dive state, the dive velocity was 0.43m/s, 0.54m/s, and 0.57m/s, respectively. By simple calculation, the gliding speed of Case 02 increased by 25.58% and 28% at the first and second dive states, respectively, compared with Case 01, and the increase became bigger when the control input was larger. After more simulations, the optimal size of the fixed wing can be obtained. It is important to note that the fixed wing in the middle of the THAUV in this paper not

only provides lift but also connects two buoyant bodies. While obtaining the maximum gliding performance, it is also necessary to pay attention to the rigid strength of the whole system to avoid the unstable failure of the system in the unstable underwater environment. In the above three cases, the gliding performance of Case 01 is not as good as that of Case 02, although Case 01 meets the system strength requirement. While the gliding performance of Case 03 is better than that of Case 02, the performance improvement is not obvious and the smaller airfoil size does not satisfy the rigid body strength requirement. Therefore, through the comparison of these three cases, the airfoil in Case 02 can not only achieve the best gliding performance but also meet the rigidity requirements of the system.

6. Conclusions

In this paper, a novel twin hybrid autonomous underwater vehicle (THAUV) that consists of a twin torpedo-shaped hull and is actuated by two buoyancy engines and two thrusters is proposed. The THAUV was designed to have faster speed generated by the two buoyancy engines and two thrusters. The two buoyancy engines on each hull and the airfoil are mainly responsible for the diving and surfacing motion, and the thrusters drive the THAUV along the horizontal plane.

In this paper, the modeling and motion simulation of a newly designed THAUV were performed and the gliding parameters of the THAUV in the vertical plane were obtained by simulation under the condition that only the buoyancy engine was operating. The effect of fixed wing size on the gliding performance of the THAUV was analyzed through the simulation comparison of three case designs.

From the cruising drag in the horizontal plane, it can be seen that the size change of the wing has little effect on the hydrodynamic drag compared with the effect of the buoyant body. The gliding parameters of the THAUV are obtained by simulation, and in the comparison of Case 01 with Case 02 it is found that the downward gliding speed of Case 02 increases by about 26% compared with that of Case 01 for the same input. It can be seen that among the three cases, Case 02 showed the best performance in gliding speed performance and in the structural strength requirements of the system.

Author Contributions: Conceptualization, H.-S.C., and J.H.; methodology, J.H.; software, J.H. and P.H.N.A.; validation, J.H., H.C., J.-H.P., K.-B.C., D.-W.J., P.H.N.A., R.Z., J.-Y.K., and D.J.; formal analysis, J.H.; investigation, J.H., J.-Y.K., and D.J.; resources, J.H. and H.-S.C.; data curation, J.H.; writing—original draft preparation, J.H.; writing—review and editing, D.-W.J., H.C., J.-H.P., K.-B.C., R.Z., H.-S.C., J.-Y.K., and D.J.; supervision, H.-S.C.; project administration, H.-S.C.; funding acquisition, H.-S.C. All authors have read and agreed to the published version of the manuscript.

Funding: This research was supported by the Unmanned Vehicles Core Technology Research and Development Program through the National Research Foundation of Korea (NRF) and Unmanned Vehicle Advanced Research Center (UVARC), funded by the Ministry of Science and ICT, the Republic of Korea, (NRF-2020M3C1C1A02086321) and (NRF-2020M3C1C1A0208632612).

Institutional Review Board Statement: Not applicable.

Informed Consent Statement: Not applicable.

Data Availability Statement: Not applicable.

Acknowledgments: The authors acknowledge all members of the Korea Maritime University Intelligent Robot & Automation Lab.

Conflicts of Interest: The authors declare no conflict of interest.

References

1. Webb, D.C.; Simonetti, P.J.; Jones, C.P. SLOCUM: An underwater glider propelled by environmental energy. *IEEE J. Ocean. Eng.* **2001**, *26*, 447–452. [CrossRef]
2. Joung, T.-H.; Sammut, K.; He, F.; Lee, S.-K. Shape optimization of an autonomous underwater vehicle with a ducted propeller using computational fluid dynamics analysis. *Int. J. Nav. Archit. Ocean. Eng.* **2012**, *4*, 44–56. [CrossRef]

3. Choi, H.; Chung, S.; Park, H.; Seo, J. Design and control of a convertible ROV. In *2012 Oceans-Yeosu*; IEEE: Piscataway, NJ, USA, 2012; pp. 1–7. [CrossRef]
4. Cadena, A.; Teran, P.; Reyes, G.; Lino, J.; Yaselga, V.; Vera, S. Development of a hybrid autonomous underwater vehicle for benthic monitoring. In Proceedings of the 4th International Conference on Control, Automation and Robotics (ICCAR), Auckland, New Zealand, 20–23 April 2018; IEEE: Piscataway, NJ, USA, 2018; pp. 437–440. [CrossRef]
5. He, M.-Q.; Williams, C.D.; Crocker, P.; Shea, D.; Riggs, N.; Bachmayer, R. A simulator developed for a twin-pod AUV, the Marport SQX-500. *J. Hydrodyn.* **2010**, *22*, 184–189. [CrossRef]
6. Makdah, A.A.R.A.; Daher, N.; Asmar, D.; Shammas, E. Three-dimensional trajectory tracking of a hybrid autonomous underwater vehicle in the presence of underwater current. *Ocean Eng.* **2019**, *185*, 115–132. [CrossRef]
7. Le, T.-L.; Hong, D.-T. Computational fluid dynamics study of the hydrodynamic characteristics of a torpedo-shaped underwater glider. *Fluids* **2021**, *6*, 252. [CrossRef]
8. Liu, Y.; Ma, J.; Ma, N.; Huang, Z. Experimental and Numerical Study on Hydrodynamic Performance of an Underwater Glider. *Math. Probl. Eng.* **2018**, *2018*, 8474389. [CrossRef]
9. Graver, J.G.; Bachmayer, R.; Leonard, N.E.; Fratantoni, D.M. Underwater glider model parameter identification. In Proceedings of the 13th International Symposium on Unmanned Untethered Submersible Technology, Durham, NH, USA, 24–27 August 2003.
10. Singh, Y.; Bhattacharyya, S.; Idichandy, V. CFD approach to modelling, hydrodynamic analysis and motion characteristics of a laboratory underwater glider with experimental results. *J. Ocean. Eng. Sci.* **2017**, *2*, 90–119. [CrossRef]
11. Ji, D.-H.; Choi, H.-S.; Kang, J.-I.; Cho, H.-J.; Joo, M.-G.; Lee, J.-H. Design and control of hybrid underwater glider. *Adv. Mech. Eng.* **2019**, *11*, 1687814019848556. [CrossRef]
12. Huang, J.; Choi, H.-S.; Jung, D.-W.; Lee, J.-H.; Kim, M.-J.; Choo, K.-B.; Cho, H.-J.; Jin, H.-S. Design and Motion Simulation of an Underwater Glider in the Vertical Plane. *Appl. Sci.* **2021**, *11*, 8212. [CrossRef]
13. Graver, J.G. Underwater Gliders: Dynamics, Control and Design. Ph.D. Thesis, Princeton University, Candidacy, NJ, USA, 2005.
14. Meyers, L.M.; Msomi, V. Hydrodynamic analysis of an underwater glider wing using ANSYS fluent as an investigation tool. *Mater. Today Proc.* **2021**, *45*, 5456–5461. [CrossRef]
15. Qin, D.; Huang, Q.; Pan, G.; Shi, Y.; Li, F.; Han, P. Numerical simulation of hydrodynamic and noise characteristics for a blended-wing-body underwater glider. *Ocean. Eng.* **2022**, *252*, 111056. [CrossRef]
16. Du, X.; Ali, N.; Zhang, L. Numerical simulations for predicting wave force effects on dynamic and motion characteristics of blended winged-body underwater glider. *Ocean. Eng.* **2021**, *235*, 109312. [CrossRef]
17. Javaid, M.Y.; Ovinis, M.; Hashim, F.B.; Maimun, A.; Ahmed, Y.M.; Ullah, B. Effect of wing form on the hydrodynamic characteristics and dynamic stability of an underwater glider. *Int. J. Nav. Archit. Ocean. Eng.* **2017**, *9*, 382–389. [CrossRef]